by the absence of puckering in the tetracobalt plane.

Isotopic Enrichment of Tetracobalt Clusters. **^{13}CO Enrichment of $Co_4(CO)_{10}(PPh)_2$.** Direct reaction of ^{13}CO with $Co_4(CO)_{10}(PPh)_2$ in benzene at temperatures up to 50 °C afforded the ^{13}CO-enriched cluster to only a small extent (~5%). Similar results were obtained using photochemical procedures. The synthesis of ^{13}CO-enriched $Co_4(CO)_{10}(PPh)_2$ was accomplished from $Co_4(CO)_{12}$ as the starting material in the following way. $Co_4(CO)_{12}$ was enriched in ^{13}CO by repeated exposure to an atmosphere of ^{13}CO. The ^{13}CO-enriched $Co_4(CO)_{12}$ (2.4 g, 0.42 mmol, with 40% ^{13}CO) was reduced with sodium amalgam in THF under an atmosphere of ^{13}CO to afford the tetracarbonylcobaltate. The solution of $Co(CO)_4^-$ was filtered over Celite and used immediately in the next step. To the filtrate was added 1.2 mL (0.0084 mol) of $PhPCl_2$ in 40 mL of THF. The reaction was stirred for 24 h at room temperature and worked up as previously described for $Co_4(CO)_{10}(PPh)_2$. The IR spectrum indicated the resulting product to be ~40% ^{13}CO enriched; yield 1.5 g (~50% based on $PhPCl_2$).

^{13}CO Enrichment of $Co_4(CO)_9[P(OMe)_3](PPh)_2$. $Co_4(CO)_9[P(OMe)_3](PPh)_2$ (0.15 g, 0.18 mmol) in 10 mL of toluene under 0.9 atm of ^{13}CO was irradiated at 355 nm (Rayonet Photochemical Reactor) for 1 week at room temperature. The cluster was recovered in essentially quantitative yield after purification by chromatography. It was found to be ~15% ^{13}CO enriched, as judged by its IR spectrum.

^{13}CO-Enriched $Co_4(CO)_8[P(OMe)_3]_2(PPh)_2$. $Co_4(CO)_{10}(PPh)_2$ (0.10 g, 0.14 mmol of ^{13}CO-enriched sample) in 7 mL of THF containing 0.1 M TBAP was electrolyzed in a bulk electrolysis cell at constant current (−1.2 V) until the conversion to the bis-substituted cluster III was complete, as observed by TLC. This procedure has already been shown to afford selectively and catalytically the bis-substituted cluster.[15] The product was isolated by column chromatography and recrystallized from hexane. The bis(phosphite) was judged to be ~40% ^{13}CO enriched by IR spectroscopy; yield 0.09 g (~71%).

^{13}CO-Enriched $Co_4(CO)_7[P(OMe)_3]_3(PPh)_2$. $Co_4(CO)_6[P(OMe)_3]_4$ (0.14 g, 0.14 mmol, of ~40% ^{13}CO-enriched complex, vide infra) in 10 mL of toluene was stirred at room temperature for 1 week under 1 atm of ^{13}CO. At that time, the quantitative conversion to the tris-substituted cluster IV was observed and the product was judged to contain ~40% ^{13}CO by IR spectroscopy.

^{13}CO-Enriched $Co_4(CO)_6[(OMe)_3]_4(PPh)_2$. To $Co_4(CO)_{10}(PPh)_2$ (0.1 g, 0.14 mmol, of ~40% ^{13}CO-enriched sample) in 20 mL of toluene was added 0.2 mL (excess) of $P(OMe)_3$. The reaction was heated at ~70 °C overnight and then allowed to cool. TLC examination revealed only the tetrakis-substitution product V to be present. The product was isolated by chromatography and found to be ~40% ^{13}CO enriched by IR spectrophotometry; yield 0.14 g (~90%).

Kinetics Studies. All kinetics runs were performed under pseudo-first-order conditions, with $P(OMe)_3$ concentrations which were greater than 10 times that of the reactant cluster. The reactions were all monitored for a minimum of 3 half-lives by following the IR absorbance of the highest energy band of the starting cluster. Plots of ln A_T vs. time afforded the pseudo-first-order rate constants, k_{obsd}, listed in Tables VII and IX. In the kinetics studies of $Co_4(CO)_{10}(PPh)_2$ and $Co_4(CO)_9[P(OMe)_3](PPh)_2$ the plots of k_{obsd} vs. the $P(OMe)_3$ concentration afforded the ligand-independent and -dependent rate constants, k_1 and k_2, respectively. The activation parameters ($\Delta H^\ddagger$ and $\Delta S^\ddagger$) were determined from the usual plots of the temperature dependences of k_1 and k_2. Error limits were calculated by using the available least-squares regression program.[60]

The energies of activation in Table XIII were calculated according to the procedure given by Shanan-Atidi and Bar-Eli.[31] Here the bridging carbonyls and terminal carbonyls were treated as unequal doublets capable of undergoing intramolecular exchange. The relative populations of the carbonyls were obtained from the integration of the slow-exchange spectrum. A variable-temperature ^{13}C NMR study allowed the determination of T_c, the coalescence temperature. At this temperature the observed chemical shift was found to be in good agreement with the weighted-average chemical shifts obtained from the slow-exchange spectrum. We have assumed that this behavior represents complete, intramolecular carbonyl scrambling about the cluster polyhedron. Through the use of the relative populations of exchanging carbonyls and the coalescence temperature, the activation energy for intramolecular carbonyl scrambling was calculated with the aid of the modified Eyring equation.[61]

Acknowledgment. We thank Dr. James D. Korp for the crystal structures in Figure 2 and the National Science Foundation and the Robert A. Welch Foundation for financial support.

Registry No. I, 58092-22-1; II, 86372-99-8; III, 100190-64-5; IV, 99918-23-7; V, 99918-24-8; $P(OMe)_3$, 121-45-9; $NaCo(CO)_4$, 14878-28-5; $PhPCl_2$, 644-97-3.

Supplementary Material Available: Lists of the bond lengths and angles of the methoxy and phenyl groups and structure factor amplitudes (21 pages). Ordering information is given on any current masthead page.

(60) Gordon, A. J.; Ford, R. A. *The Chemist's Companion: A Handbook of Practical Data, Techniques, and References*; Wiley: New York, 1976.
(61) Glasstone, S.; Laidler, K. J.; Eyring, H. *The Theory of Rate Processes*; McGraw-Hill: New York, 1941.

Contribution from the Science Research Laboratory, 3M Central Research Laboratories, St. Paul, Minnesota 55144, and Department of Chemistry, University of Minnesota, Minneapolis, Minnesota 55455

Organometallic Chemistry of Fluorocarbon Acids. Synthesis, Structure, and Solvolysis of a Sulfinate-Bridged Diruthenium Dihydride Cluster, $[(Ph_3P)_4Ru_2(\mu\text{-}H)_2(\mu\text{-}CF_3SO_2)(CO)_2]HC(SO_2CF_3)_2$

A. R. Siedle,*† R. A. Newmark,† and L. H. Pignolet‡

Received October 16, 1985

Reaction of $(Ph_3P)_3RuH_2(CO)$ with 2 equiv of the fluorocarbon acids $H_2C(SO_2CF_3)_2$ or $PhCH(SO_2CF_3)_2$ in toluene at >80 °C produces the $HC(SO_2CF_3)_2^-$ or $PhC(SO_2CF_3)_2^-$ salts of $(Ph_3P)_4Ru_2(\mu\text{-}H)_2(\mu\text{-}CF_3SO_2)(CO)_2^+$, in which the bridging hydrides were located by very high field ^{1}H NMR. The bridging bidentate CF_3SO_2 group in $[(Ph_3P)_4Ru_2(\mu\text{-}H)(\mu\text{-}CF_3SO_2)(CO)_2]HC(SO_2CF_3)_2\cdot CH_2Cl_2$ was established by single-crystal X-ray diffraction [$P\bar{1}$ (triclinic), a = 16.300 (3) Å, b = 17.783 (4) Å, c = 14.496 (2) Å, α = 92.74 (1)°, β = 90.84 (1)°, γ = 111.82 (1)°, Z = 2]. This compound reacts with acetonitrile to form salts of $(Ph_3P)_2RuH(CO)(CH_3CN)_2^+$. In the $HC(SO_2CF_3)_2^-$ derivative [$P2_1/n$ (monoclinic), a = 14.561 (3) Å, b = 16.858 (3) Å, c = 19.122 (4) Å, β = 93.55 (2)°, Z = 4], d(Ru–N, trans to CO) is 2.108 (5) Å while d(Ru–N, trans to H) is 2.163 (5) Å and one of the acetonitrile ligands rapidly exchanges with CD_3CN.

Introduction

We have previously described the organometallic chemistry of the novel fluorochemical acids **1** and **2**[1] and showed how these compounds can be used in the absence of donor solvents to synthesize cationic metal hydrides that contain the noncoordinating counterions $HC(SO_2CF_3)_2^-$ and $PhC(SO_2CF_3)_2^-$.[2,3] High

† 3M Central Research Laboratories.
‡ University of Minnesota.

(1) Koshar, R. J.; Mitsch, R. A. *J. Org. Chem.* **1973**, *38*, 3358.
(2) Siedle, A. R.; Newmark, R. A.; Pignolet, L. H.; Howells, R. D. *J. Am. Chem. Soc.* **1984**, *106*, 1510.

0020-1669/86/1325-1345$01.50/0

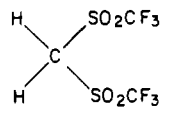

1

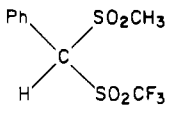

2

Brønsted acidity is exhibited by **1** and **2** since the C–H bonds are readily ionized. However, both bis(perfluoroalkylsulfonyl)alkanes and their conjugate bases have high thermodynamic stability with regard to rupture of the C–S, S–O, and C–F bonds. We now report the first degradative chemical reaction of **1** and **2** in which a CF_3SO_2 fragment emerges as an unusual bridging ligand spanning the two metal centers in $[(Ph_3P)_4Ru_2(\mu\text{-}H)_2(\mu\text{-}CF_3SO_2)(CO)_2]^+$. This paper describes the characterization of this cation by X-ray crystallography and ultrahigh-field NMR spectroscopy and a remarkably specific solvolysis by acetonitrile that produces $(Ph_3P)_2Ru(H)(CO)(CH_3CN)_2^+$.

Results and Discussion

In an earlier survey of the protonation chemistry of the hydrides of iron, ruthenium, and osmium, we found that the reaction of $(Ph_3P)_3RuH_2(CO)$ with 1 equiv of **1** in toluene at room temperature produced hydrogen and $[(Ph_3P)_3RuH(CO)]HC(SO_2CF_3)_2{\cdot}2C_6H_5CH_3$. When the ruthenium dihydride is instead allowed to react with 2 equiv of $H_2C(SO_2CF_3)_2$ in toluene at ≥80 °C, $[(Ph_3P)_4Ru_2(\mu\text{-}H)_2(\mu\text{-}CF_3SO_2)(CO)_2]HC(SO_2CF_3)_2$ (**3**) is formed in 45% yield. When the fluorocarbon acid $PhCH(SO_2CF_3)_2$ is used instead, the yield of the analogous $PhC(SO_2CF_3)_2^-$ salt, **4**, is 85%. The trifluoromethanesulfinato-bridged compound **3** is a brown, air-stable crystalline solid. Chloroform solutions show maxima in the electronic spectrum at 312 (log ε 4.31), 355 (4.21), 414 (3.84), and 455 (3.53) nm. The solid is thermochromic and appears orange above liquid-nitrogen temperature, but no phase transition between +10 and −160 °C was detected by differential scanning calorimetry. The infrared spectrum shows a single, strong C–O stretching band at 1980 cm^{-1} and strong absorptions in the 1100–1200-cm^{-1} region due to the CF_3SO_2 groups; there are no bands clearly attributable to Ru–H vibrations. We shall anticipate the results of the X-ray diffraction experiments and describe the NMR spectra of **3** in terms of its

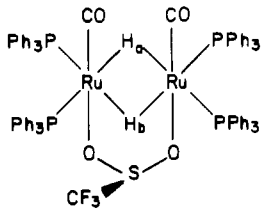

3

established structure, in which the bridging hydrides, not located in the electron density maps but clearly revealed by the ^1H NMR spectra, are shown.

The ^{19}F NMR spectrum of **3** in dichloromethane shows two singlet resonances at δ −81.5 and −82.2 in a 2:1 ratio. The −81.5 ppm signal is due to the $HC(SO_2CF_3)_2^-$ ion, as is the ^1H resonance at δ 3.84, and the −82.2 ppm peak is assigned to the bridging CF_3SO_2 group. The ^{19}F NMR spectrum of **4** in acetone-d_6 shows a singlet at δ −77.8 [2 F, $PhC(SO_2CF_3)_2^-$] and −81.8 (1 F, $\mu\text{-}CF_3SO_2^-$); there is no signal near δ 3.8 in this compound. The $^{31}P\{^1H\}$ NMR spectrum of **3** (and **4**) shows two peaks of equal area at δ 39.9 and 38.0 with incompletely resolved fine structure due to coupling between chemically equivalent nuclei in the AA′BB′ spin system. The ^{13}C NMR spectrum reveals a broad resonance at δ 203.1 due to the Ru–CO groups. The 200-MHz ^1H NMR spectrum displays a complex hydride multiplet near −11 ppm, which was initially uninterpretable, but it established that the Ph_3P:$HC(SO_2CF_3)_2^-$ hydride ratio is 4:1:2. However, the ^1H NMR spectrum obtained at 600 MHz (Figure 1) is first order and dramatically serves to establish the number and location of

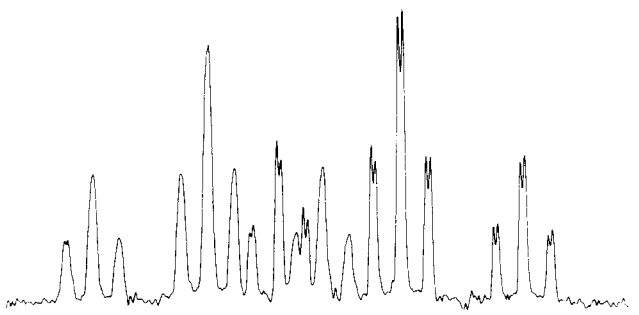

Figure 1. 600-MHz ^1H NMR spectrum (hydride region) of **3**. Chemical shifts and coupling constants are given in the text.

the hydride ligands. This very high field spectrum reveals two overlapping triplets of triplets of doublets separated by 0.14 ppm. Two such patterns appear because the SCF_3 portion of the CF_3SO_2 bridge is canted and displaced away from the mirror plane passing through the two ruthenium atoms and the two carbonyl ligands (vide infra), thus making H_a and H_b nonequivalent. One hydride has δ −11.11; it is split into a triplet of triplets by couplings of 52.3 Hz to two trans Ph_3P groups and 11.7 Hz to two cis Ph_3P groups. Similarly, the other bridging hydride, H_b, has δ −10.97 with J_{P-H}(trans) = 48.2 Hz and J_{H-P}(cis) = 11.4 Hz. There is a 2.5-Hz coupling between H_a and H_b. Spin coupling of the two hydrides to two pairs of ^{31}P nuclei serves to uniquely locate these protons in bridging positions between the two ruthenium atoms.

Solvolysis of $[(Ph_3P)_4Ru_2(\mu\text{-}H)_2(\mu\text{-}CF_3SO_2)(CO)_2]HC(SO_2CF_3)_2$. Solutions of **3** in acetonitrile are initially brown but are bleached after several days at room temperature; the decolorization is accelerated by heating. This is due to solvolysis by acetonitrile, which proceeds according to eq 1. The process

$$[(Ph_3P)_4Ru_2(\mu\text{-}H)_2(\mu\text{-}CF_3SO_2)(CO)_2]HC(SO_2CF_3) + 4CH_3CN \rightarrow 2(Ph_3P)_2RuH(CO)(CH_3CN)_2^+ + CF_3SO_2^- + HC(SO_2CF_3)_2^- \quad (1)$$

involves rupture of the Ru–Ru and Ru–H–Ru bonds. The bridging CF_3SO_2 group emerges as the trifluoromethanesulfinate ion, and when the solvolysis is carried out in an NMR tube, a singlet ^{19}F resonance at δ −87.2 due to this ion is observed; cf. δ −87.5 for $Na^+CF_3SO_2^-$ in acetone. Although cluster solvolysis is quantitative with respect to the mononuclear ruthenium hydride, the yield of $CF_3SO_2^-$ is not, probably because of facile hydrolysis by adventitious water to give HCF_3, SO_2, and OH^-. Crystallization of the reaction mixture from methylene chloride–cyclohexane gives, as the less soluble fraction, $[(Ph_3P)_2RuH(CO)(CH_3CN)_2]CF_3SO_2$ (**5**), δ(^{19}F) −87.2. Crystallization of the solvolysis products from ethanol provides $[(Ph_3P)_2RuH(CO)(CH_3CN)_2]HC(SO_2CF_3)_2$ (**6**), the perchlorate analogue of which has been synthesized by the reaction of $(Ph_3P)_3RuHCl(CO)$ with silver perchlorate in acetonitrile.[4] The infrared spectrum of **6** shows ν_{CO} at 1940 cm^{-1} (s) and ν_{Ru-H} at 1980 cm^{-1} (m). The ^{19}F and ^{31}P NMR spectra show single resonances at δ −81.5 and 46.4, respectively; the narrow-band ^1H-coupled ^{31}P NMR spectrum reveals an 18-Hz doublet, indicating that only one hydride is present. The ^1H NMR spectrum is unusual and informative. In CD_3CN, the Ru–H proton appears as a triplet at −13.0 ppm; J_{P-H} = 18 Hz. Two methyl resonances due to nonequivalent coordinated acetonitrile ligands occur at δ 1.69 and 1.36 in $CDCl_3$. In CD_3CN, one of these ligands, likely that trans to the hydride (vide infra) and having the downfield chemical shift, is more labile than the other and exchanges with CD_3CN within sample preparation time. When solutions of **6** in CD_3CN are warmed, the 1.36 ppm signal, due to the less labile acetonitrile, also disappears due to incorporation of CD_3CN into the ruthenium coordination sphere. Solvolysis of $[(Ph_3P)_2RuH(CO)(CH_3CN)(CD_3CN)]PhC(SO_2CF_3)_2$ (**6a**) in CD_3CN was followed by ^1H NMR spectros-

(3) Siedle, A. R.; Newmark, R. A.; Pignolet, L. H. *Organometallics* **1984**, *3*, 855.

(4) Cavit, B. E.; Grundy, K. R.; Roper, W. R. *J. Chem. Soc., Chem. Commun.* **1972**, 60. These workers also noted enhanced lability of one of the acetonitrile ligands.

copy. The reaction producing $[(Ph_3P)_2RuH(CO)(CD_3CN)_2]$-$PhC(SO_2CF_3)_2$ is first order in the cationic ruthenium compound and has a pseudo-first-order rate constant of 9.3×10^{-4} s at 27 °C. The long-wavelength bands at 405 and 455 nm in the starting cluster are absent in the mononuclear solvolysis product, suggesting that these absorptions are associated with a $Ru_2(\mu\text{-}H)_2(\mu\text{-}CF_3SO_2)$ chromophore, **7**. The cluster degradation reaction shown in eq

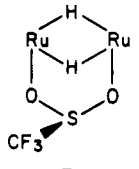

7

1 is singularly specific in that it appears to be confined to organonitriles. Analogous cleavage processes have not been observed with other Lewis bases such as pyridine, triphenylphosphine, or *tert*-butyl isocyanade. Similarly, we have not been able to remove the CF_3SO_2 bridge with oxidizing agents such as *tert*-butyl hydroperoxide, trimethylamine *N*-oxide, or iodosobenzene. Reaction of **3** with $PPN^+Co(CO)_4^-$ in acetonitrile merely gave the metathesis product $[(Ph_3P)_4Ru_2(\mu\text{-}H)_2(\mu\text{-}CF_3SO_2)(CO)_2]Co(CO)_4$ (**8**), whose infrared spectrum was a composite of the two carbonyl-containing species present.

Nucleophilic attack on the Ru–H–Ru bridges is observed with strong hydride donors. Reaction of **4** in 1,2-dimethoxyethane (glyme) with lithium triethylborohydride affords a dark purple microcrystalline solid formulated as $(Ph_3P)_4Ru_2H_2(\mu\text{-}H)$-$(CF_3SO_2)(CO)_2$ (**9**). The electronic spectrum of this material reveals absorptions at 380, 410, 490, 550, and 720 nm. The infrared spectrum contains bands at 1945 (s, Ru–CO), 1900 (m, Ru–H), and 1025 (m, CH_2–O–CH_3) cm^{-1}, and the spectrum of the material produced by using $LiB(C_2H_5)_3D$ as a deuteride source is essentially identical. ^{19}F NMR analysis of the reaction mixture from which **9** separated shows that $PhC(SO_2CF_3)_2^-$, δ −78.9, is formed as a coproduct in the reaction.

Characterization of the new, neutral ruthenium hydride cluster **9** is hampered by its low solubility in nonreactive organic liquids. The best solvent for NMR experiments was CD_2Cl_2; spectra were obtained at −30 °C, above which the rate of decomposition is significant and below which solubility is uselessly low. The ^1H NMR data do establish the presence of 0.5 equiv. of 1,2-dimethoxyethane solvate and show a complex multiplet in the hydride region at δ −10.5. As decomposition (or more likely reaction with the CD_2Cl_2, since **9** should be a good hydride donor) proceeds, a peak at δ −11.0 grows in due to regeneration of the starting $[(Ph_3P)_4Ru_2(\mu\text{-}H)_2(\mu\text{-}CF_3SO_2)(CO)_2]^-$ ion. We suggest that **9** arises by nucleophilic attack at the Ru–$(\mu$-H$)_2$–Ru unit. The entering hydride or deuteride adopts a bridging position between the two ruthenium atoms and displaces the original bridging hydrides into terminal positions (eq 2). This logically accounts

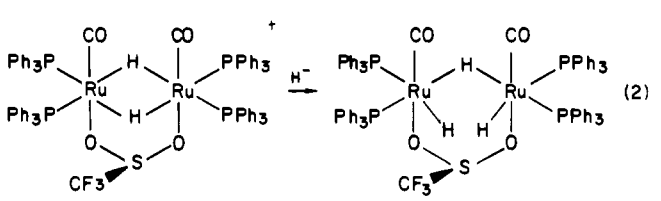

(2)

for the striking absence of terminal Ru–D stretching bands in $(Ph_3P)_4Ru_2(\mu\text{-}D)H_2(\mu\text{-}CF_3SO_2)(CO)_2$ made from **3** and LiB-$(C_2H_5)_3D$ as well as for facile reversion to $[(Ph_3P)_4Ru_2(\mu\text{-}H)_2$-$(\mu\text{-}CF_3SO_2)(CO)_2]^-$ by loss of D^-.

Solid-State Structure of 3. The structure of $[(Ph_3P)_4Ru_2(\mu$-$H)_2(\mu\text{-}CF_3SO_2)(CO)_2]HC(SO_2CF_3)_2\cdot CH_2Cl_2$ was determined by single-crystal X-ray diffraction in order to establish the nature of the CF_3SO_2 bridge whose existence was implied by the ^{19}F NMR spectra and chemical analyses. Crystals of a dichloromethane solvent were grown by diffusion of toluene into a solution of the compound in dichloromethane. The chlorinated hydrocarbon is present in the lattice as solvent of crystallization and is easily removed by pumping or by allowing the crystals to stand in air. An ORTEP view of the cation of **3** is shown in Figure 2, and important distances and angles are given in Table I. Crystal data, atomic positional parameters, etc. are presented in Table II and as supplementary material.[5]

Table I. Selected Distances (Å) and Angles (deg) in the Cation of $[(Ph_3P)_4Ru_2(\mu\text{-}H)_2(\mu\text{-}CF_3SO_2)(CO)_2]HC(SO_2CF_3)_2\cdot CH_2Cl_2$ (**3**)[a]

		Distances	
Ru1–Ru2	2.773 (1)	O3–S1	1.494 (7)
Ru1–P1	2.385 (2)	O4–S1	1.524 (7)
Ru1–P2	2.349 (2)	O3–S1′	1.508 (8)
Ru1–C2	1.821 (7)	O4–S1′)	1.513 (8)
Ru1–O3	2.163 (4)	S1–C3	1.80 (3)
Ru2–P3	2.387 (2)	S1′–C3′	1.67 (3)
Ru2–P4	2.358 (2)	C3–F1	1.35 (3)
Ru2–C1	1.827 (7)	C3–F2	1.30 (3)
Ru2–O4	2.173 (4)	C3–F3	1.30 (3)
C1–O1	1.14 (1)	C3′–F1	1.28 (3)
C2–O2	1.16 (1)	C3′–F2	1.31 (3)
		C3′–F3′	1.27 (3)
		Angles	
Ru2–Ru1–P1	129.14 (5)	C2–Ru1–O3	175.5 (2)
Ru2–Ru1–P2	131.48 (5)	C1–Ru2–O4	175.0 (2)
Ru2–Ru1–C2	93.03 (6)	C2–Ru1–P1	88.1 (2)
Ru2–Ru1–O3	85.76 (7)	C2–Ru1–P2	92.2 (2)
Ru1–Ru2–P3	130.14 (5)	C1–Ru2–P3	88.4 (2)
Ru1–Ru2–P4	129.88 (5)	C1–Ru2–P4	92.1 (2)
Ru1–Ru2–C1	93.15 (6)	Ru1–O3–S1	117.0 (3)
Ru1–Ru2–O4	86.25 (6)	Ru1–O3–S1′	119.0 (3)
P1–Ru1–P2	99.21 (6)	Ru2–O4–S1	117.6 (3)
P3–Ru2–P4	99.79 (6)	Ru2–O4–S1′	116.2 (3)
O3–Ru1–P1	96.1 (1)	O3–S1–O4	110.2 (3)
O3–Ru1–P2	85.3 (1)	O3–S1′–O4	110.1 (3)
O4–Ru2–P3	95.8 (1)	O3–S1–C3	98.8 (9)
O4–Ru4–P4	84.5 (1)	O3–S1–C3′	110 (1)
Ru1–C2–O2	176.5 (7)	O4–S1–C3	97.4 (9)
Ru2–C1–O1	176.9 (7)	O4–S1–C3′	111 (1)

[a] Primed atoms belong to the disordered SO_2CF_3 group (see text).

The structure of the cation of **3** is bimetallic and consists of two $Ru(Ph_3P)_2(CO)$ units bridged by a CF_3SO_2 group. The two bridging hydrides were not located in the electron density maps and are not shown in Figure 2. However, as explained above, their position as bridging ligands between the two ruthenium atoms approximately trans to the Ru–P vectors follows clearly from the high-field ^1H NMR data and, indirectly, from the X-ray data below. The ion consists of two approximately octahedral $(Ph_3P)_2Rh(CO)(O-)$ units sharing a common H–H edge. The distance between the two ruthenium centers is 2.733 (1) Å. This is comparable to *d*(Ru–Ru) values of 2.811 (4) and 2.540 (1) Å in $Ru_2H_4[P(CH_3)_3]_6$ and $Ru_2H_3[P(CH_3)_3]_6^+$, respectively,[6] and makes reasonable the assumption of closed, two-electron, three-center bonds in the Ru_2H_2 unit, which would lead to an 18-electron configuration around each metal atom.

The P1–Ru1–P2 and P3–Ru2–P4 angles are 99.21 (6) and 99.79 (6)°, respectively, indicating that the bridging hydrides are stereochemically active in that they exert an influence on the coordination geometry around ruthenium. The ruthenium–phosphorus contacts fall into two sets: Ru1–P1 and Ru2–P3, 2.385 (2) and 2.387 (2) Å, respectively; and Ru1–P2 and Ru2–P4, 2.349 (2) and 2.358 (2) Å, respectively. No significance is attached to the difference between these two sets. The average Ru–P separation, however, is 2.379 (2) Å, which appears slightly large in comparison with, for example the 2.206–2.361-Å range in $(Ph_3P)_3RuHCl$.[7] The trans effect of the two bridging hydrides is probably responsible for this lengthening. The two RuP_2 planes are somewhat twisted relative to one another, and the dihedral angle between the P1,P2,Ru1 and P3,P4,Ru2 planes is 19.5°.

(5) See paragraph at end of paper regarding supplementary material.
(6) Jones, R. A.; Wilkinson, G.; Colquohon, I. McFarlane, W.; Galas, A. M. R.; Hursthouse, M. B. *J. Chem. Soc., Dalton Trans.* **1980**, 2480.
(7) Skapski, A. C.; Troughton, P. G. H. *Chem. Commun.* **1968**, 1230.

Table II. Positional Parameters and Their Estimated Standard Deviations for $[(Ph_3P)_4Ru_2(\mu\text{-}H)_2(\mu\text{-}CF_3SO_2)(CO)_2]HC(SO_2CF_3)_2\cdot CH_2Cl_2$ (**3**)[a]

atom	x	y	z	B, Å²	atom	x	y	z	B, Å²
Ru1	0.24056 (5)	0.24045 (5)	0.14645 (6)	1.87 (2)	C2K	0.1266 (7)	0.2165 (7)	0.5515 (8)	3.6 (2)*
Ru2	0.30673 (5)	0.21021 (5)	0.31217 (6)	1.91 (2)	C2L	0.2119 (7)	0.3610 (7)	0.4106 (8)	3.5 (2)*
S1	0.4253 (4)	0.3666 (3)	0.2130 (4)	2.8 (1)	C3A	0.0028 (8)	0.2033 (7)	−0.1384 (9)	4.4 (3)*
S1′	0.3787 (3)	0.3920 (3)	0.2601 (4)	2.4 (1)	C3B	0.2295 (8)	0.5308 (7)	0.1538 (9)	4.4 (3)*
Cl1	0.7119 (6)	0.1551 (5)	0.1424 (9)	16.0 (4)	C3C	−0.0155 (8)	0.1838 (7)	0.3496 (9)	4.2 (3)*
Cl2	0.8221 (7)	0.2863 (7)	0.0697 (9)	38.9 (4)	C3D	0.5340 (8)	0.2277 (8)	0.045 (1)	4.8 (3)*
S3	0.1599 (3)	0.7470 (4)	0.3328 (4)	9.3 (2)	C3E	0.2685 (9)	0.0416 (8)	−0.177 (1)	5.2 (3)*
S4	0.0425 (4)	0.5797 (3)	0.2986 (4)	10.2 (2)	C3F	0.2878 (8)	0.4533 (7)	−0.1013 (9)	3.9 (3)*
P1	0.1211 (2)	0.2849 (2)	0.1196 (2)	2.34 (6)	C3	0.462 (1)	0.471 (1)	0.253 (2)	3.4 (6)
P2	0.2897 (2)	0.2409 (2)	−0.0051 (2)	2.30 (6)	C3′	0.493 (1)	0.463 (1)	0.223 (1)	3.6 (6)
P3	0.4073 (2)	0.1436 (2)	0.3408 (2)	2.53 (6)	C3G	0.481 (1)	−0.004 (1)	0.159 (1)	7.6 (4)*
P4	0.2892 (2)	0.2527 (2)	0.4648 (2)	2.18 (6)	C3H	0.6439 (9)	0.3194 (9)	0.291 (1)	5.8 (4)*
F1	0.4786 (6)	0.5187 (4)	0.1803 (6)	7.7 (3)	C3I	0.2917 (9)	−0.0542 (8)	0.494 (1)	5.3 (3)*
F2	0.5355 (6)	0.4945 (5)	0.3013 (6)	8.1 (3)	C3J	0.5346 (7)	0.3278 (7)	0.5876 (8)	3.8 (3)*
F3	0.403 (1)	0.4908 (9)	0.298 (1)	6.7 (5)	C3K	0.0508 (9)	0.1621 (8)	0.596 (1)	5.4 (3)*
F3′	0.529 (1)	0.422 (1)	0.176 (1)	6.8 (5)	C3L	0.1998 (7)	0.4357 (7)	0.4132 (8)	3.4 (2)*
F4	−0.3259 (8)	0.1762 (7)	0.676 (1)	13.1 (4)	C4B	0.1840 (9)	0.5567 (8)	0.091 (1)	5.1 (3)*
F5	−0.269 (1)	0.2433 (8)	0.7993 (8)	15.3 (5)	C4C	−0.0530 (9)	0.2405 (8)	0.379 (1)	5.4 (3)*
F6	0.2802 (7)	0.6917 (8)	0.316 (1)	17.8 (6)	C4D	0.5900 (9)	0.2962 (8)	0.002 (1)	5.2 (3)*
F7	−0.080 (1)	0.4964 (8)	0.397 (1)	16.7 (6)	C4E	0.1752 (8)	0.0043 (8)	−0.1906 (9)	4.5 (3)*
F8	−0.1032 (8)	0.592 (1)	0.348 (1)	19.3 (5)	C4F	0.2596 (8)	0.4316 (7)	−0.1947 (9)	4.5 (3)*
F9	−0.0181 (8)	0.6085 (9)	0.4556 (8)	12.9 (5)	C4G	0.407 (1)	−0.0384 (9)	0.100 (1)	6.3 (4)*
O1	0.1582 (5)	0.0540 (5)	0.3235 (6)	4.2 (2)	C4	0.259 (1)	0.764 (1)	0.282 (1)	11.8 (6)
O2	0.1164 (5)	0.0699 (4)	0.1195 (6)	3.8 (2)	C4H	0.700 (1)	0.3068 (9)	0.356 (1)	6.3 (4)*
O3	0.3413 (4)	0.3598 (4)	0.1643 (5)	2.6 (2)	C4I	0.3288 (9)	−0.0263 (8)	0.583 (1)	5.6 (3)*
O4	0.4065 (4)	0.3304 (4)	0.3071 (5)	2.5 (2)	C4J	0.5178 (8)	0.3031 (7)	0.6780 (9)	4.7 (3)*
O5	0.164 (1)	0.8271 (7)	0.293 (1)	17.3 (6)	C4K	0.045 (1)	0.0832 (9)	0.607 (1)	6.1 (4)*
O6	−0.1088 (9)	0.439 (1)	0.638 (2)	20.1 (6)	C4L	0.2519 (8)	0.4998 (7)	0.4706 (9)	4.1 (3)*
O7	−0.006 (1)	0.529 (1)	0.221 (1)	19.3 (7)	C4A	−0.0644 (8)	0.1315 (8)	−0.1199 (9)	4.6 (3)*
O8	−0.1670 (8)	0.2639 (8)	0.5761 (7)	9.0 (4)	C5D	0.5567 (9)	0.3455 (8)	−0.044 (1)	5.0 (3)*
C	0.804 (2)	0.226 (2)	0.142 (3)	16 (1)*	C5E	0.1198 (8)	0.0394 (7)	−0.1480 (9)	4.0 (3)*
C1L	0.2767 (6)	0.3522 (6)	0.4656 (7)	2.5 (2)*	C5F	0.2405 (8)	0.3528 (7)	−0.2310 (9)	4.1 (3)*
C1A	0.0450 (7)	0.2287 (6)	0.0256 (7)	2.7 (2)*	C5G	0.3339 (8)	−0.0189 (7)	0.1127 (9)	4.6 (3)*
C1B	0.1434 (7)	0.3910 (6)	0.1036 (7)	2.8 (2)*	C5H	0.674 (1)	0.2459 (9)	0.415 (1)	6.0 (4)*
C1E	0.2469 (7)	0.1447 (6)	−0.0757 (7)	2.7 (2)*	C5I	0.3899 (9)	0.0503 (8)	0.600 (1)	5.3 (3)*
C1F	0.2774 (6)	0.3145 (6)	−0.0817 (7)	2.6 (2)*	C5	−0.046 (1)	0.565 (1)	0.378 (1)	7.9 (5)
C1G	0.4061 (7)	0.0723 (6)	0.2432 (7)	2.9 (2)*	C5J	0.4333 (8)	0.2641 (7)	0.7036 (9)	4.3 (3)*
C1H	0.5238 (7)	0.2051 (6)	0.2517 (8)	2.8 (2)*	C5K	0.1098 (9)	0.0552 (8)	0.579 (1)	5.6 (3)*
C1C	0.0506 (6)	0.2659 (6)	0.2214 (7)	2.7 (2)*	C5L	0.3171((8)	0.4898 (7)	0.5256 (9)	4.5 (3)*
C1D	0.4078 (7)	0.2635 (6)	−0.0007 (7)	2.6 (2)*	C5A	−0.0791 (8)	0.1057 (7)	−0.0295 (9)	4.1 (3)*
C1	0.2166 (7)	0.1133 (6)	0.3207 (7)	2.6 (2)	C5B	0.1171 (9)	0.5028 (8)	0.034 (1)	5.1 (3)*
C1I	0.3820 (7)	0.0757 (6)	0.4363 (8)	3.0 (2)*	C5C	−0.0372 (9)	0.3098 (8)	0.330 (1)	5.5 (3)*
C1K	0.1907 (7)	0.1884 (6)	0.5218 (7)	2.7 (2)*	C6J	0.3621 (7)	0.2460 (6)	0.6410 (8)	3.4 (2)*
C1J	0.3790 (6)	0.2704 (6)	0.5486 (7)	2.3 (2)*	C6K	0.1862 (8)	0.1083 (7)	0.5342 (9)	4.3 (3)*
C2A	0.0592 (7)	0.2539 (6)	−0.0660 (8)	3.4 (2)*	C6L	0.3316 (7)	0.4147 (7)	0.5252 (8)	3.6 (2)*
C2B	0.2099 (7)	0.4465 (6)	0.1630 (8)	3.4 (2)*	C6E	0.1554 (7)	0.1080 (7)	−0.0895 (8)	3.4 (2)*
C2C	0.0371 (7)	0.1967 (7)	0.2712 (8)	3.2 (2)*	C6F	0.2496 (7)	0.2941 (6)	−0.1740 (8)	3.4 (2)*
C2D	0.4416 (8)	0.2134 (7)	0.0447 (9)	4.1 (3)*	C6A	−0.0243 (7)	0.1559 (6)	0.0437 (8)	3.3 (2)*
C2E	0.3034 (8)	0.1125 (7)	−0.1180 (9)	4.2 (3)*	C6B	0.0947 (8)	0.4189 (7)	0.0398 (8)	3.8 (3)*
C2F	0.2957 (7)	0.3938 (6)	−0.0448 (8)	3.1 (2)*	C6C	0.0145 (8)	0.3229 (7)	0.2500 (9)	3.9 (3)*
C2G	0.4815 (9)	0.0519 (8)	0.231 (1)	5.0 (3)*	C6G	0.3324 (8)	0.0364 (7)	0.1837 (9)	3.7 (3)*
C2H	0.5539 (8)	0.2681 (7)	0.2892 (9)	4.2 (3)*	C6H	0.5843 (8)	0.1925 (8)	0.4155 (9)	4.8 (3)*
C2I	0.3201 (8)	−0.0016 (7)	0.4200 (9)	4.0 (3)*	C6I	0.4169 (8)	0.1040 (7)	0.5268 (9)	3.9 (3)*
C2	0.1626 (6)	0.1370 (6)	0.1289 (7)	2.6 (2)	C6D	0.4646 (8)	0.3300 (7)	−0.0452 (9)	3.9 (3)*
C2J	0.4655 (7)	0.3116 (6)	0.5223 (8)	3.2 (2)*	C34	−0.060 (2)	0.340 (1)	0.725 (1)	17.3 (7)

[a] Primed atoms refer to the disordered SO_2CF_3 group (see text). Values marked with an asterisk indicate that the atoms were refined isotropically. Anisotropically refined atoms are given in the form of the isotropic equivalent thermal parameter defined as $^4/_3[a^2B(11) + b^2B(22) + c^2B(33) + ab(\cos\gamma)B(12) + ac(\cos\beta)B(13) + bc(\cos\alpha)B(23)]$.

The trifluoromethanesulfinate unit is bidentate, and it forms a bridge between Ru1 and Ru2 in which the axial Ru–O contacts, Ru2–O4 and Ru1–O3, are 2.173 (4) and 2.163 (4) Å, respectively. The Ru1–Ru2–O3–O4–S1 framework forms a pentagonal envelope folded along the O3–O4 vector. The Ru_2O_2 portion is essentially planar with maximum displacements from the weighted least-squares planes of −0.07 Å at O3 and +0.07 Å at O4. Least-squares planes are included as supplementary material. The CF_3S "flap" portion of this envelope is disordered in that it lies on both sides of the approximate mirror plane passing through Ru1, Ru2, O3, O4, C1, and C2. The disorder was modeled by using a 0.5 occupancy for the two conformations in the solid state. Only one conformation is shown in Figure 2. The other conformer of the disordered CF_3S group is indicated with primed atoms. The dihedral angles between the Ru1,Ru2,O3,O4 plane and the O3,O4,S1 and O3,O4,S1′ planes are 45.0 and 44.5°, respectively. The four S–O distances, S1–O3, S1′–O3, S1–O4, and S1′–O4, are 1.494 (7), 1.508 (8), 1.524 (7), and 1.513 (8) Å, respectively, with an average value of 1.510 (7) Å. We have been unable to find as precedent a crystallographically characterized compound containing an alkanesulfinate ligand. Therefore we will use, for purposes of comparison, structural information on sulfur dioxide complexes.[8] Wilson and Ibers[9] prepared $(Ph_3P)_2RuCl(NO)(OS\text{–}SO_2)$ in which d(Ru–O) is 2.144 (6) Å and the S–O distances are 1.504 (5) and 1.459 (5) Å, comparable to those in **3**.

Distances and angles in the $HC(SO_2CF_3)_2^-$ anion and CH_2Cl_2 solvate are normal and are given as supplementary material.[5] Both of these molecules were found to be loosely bound and have large thermal parameters.

(8) Kubas, G. J. *Inorg. Chem.* **1979**, *18*, 182.
(9) Wilson, R. D.; Ibers, J. A. *Inorg. Chem.* **1978**, *17*, 2134.

Table III. Selected Distances (Å) and Angles (deg) in the Cation of $[(Ph_3P)_2RuH(CO)(CH_3CN)_2]HC(SO_2CF_3)_2$ (**6**)

	Distances		
Ru–P1	2.372 (2)	C–O	1.153 (6)
Ru–P2	2.367 (2)	N1–C1	1.130 (7)
Ru–C	1.824 (7)	N2–C3	1.128 (7)
Ru–N1	2.108 (5)	C1–C2	1.484 (8)
Ru–N2	2.163 (5)	C3–C4	1.49 (1)
Ru–H	1.32 (6)		
	Angles		
P1–Ru–P2	170.42 (6)	N1–Ru–N2	87.9 (2)
P1–Ru–C	89.1 (2)	N1–Ru–C	174.3 (2)
P1–Ru–N1	90.5 (2)	N1–Ru–H	88 (2)
P1–Ru–N2	96.2 (1)	N2–Ru–C	97.8 (2)
P1–Ru–H	85 (1)	N2–Ru–H	175 (2)
P2–Ru–C	89.5 (2)	C–Ru–H	87 (2)
P2–Ru–N1	89.9 (1)	Ru–C–O	177.9 (6)
P2–Ru–N2	93.3 (1)	Ru–N1–C1	177.0 (6)
P2–Ru–H	86 (1)	Ru–N2–C3	177.0 (5)
		N1–C1–C2	177.9 (7)
		N2–C3–C4	175.2 (9)

Solid-State Structure of 6. The compound $[(Ph_3P)_2RuH(CO)(CH_3CN)_2]HC(SO_2CF_3)_2$ crystallizes as an ionic solid with no close intermolecular contacts between the cation and $HC(SO_2CF_3)_2^-$ anion. Figure 3 shows an ORTEP drawing of the $(Ph_3P)_2RuH(CO)(CH_3CN)_2^+$ cation and the numbering system used in its description. Selected bond distances and angles are given in Table III, and atomic coordinates and anisotropic thermal parameters are found in Table IV and as supplementary material. The ruthenium atom lies at the center of an approximately octahedral array of ligands. The hydride atom was located, and its positional parameters were refined. Distortions from idealized geometry are apparent in that the triphenylphosphine groups are tipped so that the P1–Ru–P2 angle is 170.42 (6)°. The N2–Ru–C angle is 97.8 (2)°, and all cis angles involving the hydride are less than 90°, so slight movement of the large organic ligands toward the position occupied by the smaller hydride is evident. Both Ru–P separations are the same within experimental error, and $d(Ru–P)_{av}$ is 2.369 (2) Å. The Ru–H and Ru–CO distances are 1.32 (6) and 1.824 (7) Å, respectively, and the H–Ru–C angle is 87 (2)°.

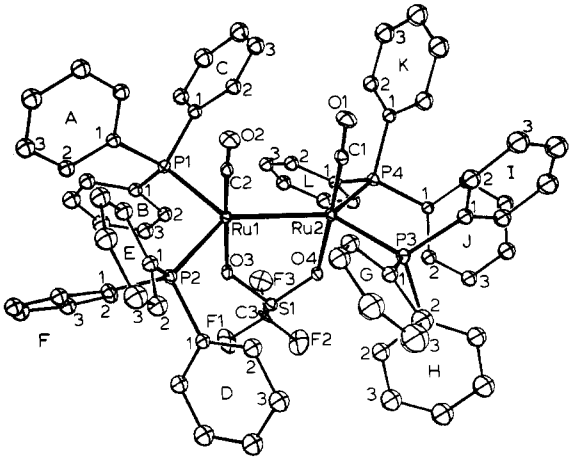

Figure 2. ORTEP drawing of the molecular structure of the cation, $[(Ph_3P)_4Ru_2(\mu\text{-}H)_2(\mu\text{-}CF_3SO_2)(CO)_2]^+$, of **3**. Ellipsoids are drawn with 35% probability boundaries.

The geometry of the two acetonitrile ligands is essentially the same with $d(C–N)_{av}$ = 1.129 (7) Å, $d(C–C)_{av}$ = 1.484 (8) Å, and $\angle(C–N–Ru)_{av}$ = 177.0 (6)°. A striking feature is the marked inequivalence of the ruthenium–nitrogen distances: Ru–N1, involving the acetonitrile molecule trans to the carbonyl group, is 2.108 (5) Å while Ru–N2, involving the acetonitrile ligand trans to hydride, is 2.163 (5) Å. This difference in Ru–N bond lengths corresponds to a structural trans effect that is reflected in the greater kinetic lability of one of the coordinated acetonitrile ligands toward displacement by CD_3CN (vide supra).

Experimental Section

NMR spectra were recorded on a 4.7T Varian XL-200 instrument; chemical shifts are expressed with respect to internal $(CH_3)_4Si$ (^1H and

Table IV. Positional Parameters and Their Estimated Standard Deviations for $[(Ph_3P)_2RuH(CO)(CH_3CN)_2]HC(SO_2CF_3)_2$ (**6**)[a]

atom	x	y	z	B, Å²	atom	x	y	z	B, Å²
Ru	0.48053 (5)	0.20129 (4)	0.15169 (3)	3.55 (1)	C2E	0.6474 (7)	−0.0313 (6)	0.2379 (5)	7.2 (3)*
S1	0.0759 (2)	0.2010 (2)	0.1063 (1)	7.38 (7)	C2F	0.4383 (6)	−0.0167 (6)	0.3073 (5)	6.3 (2)*
S2	−0.0558 (2)	0.1398 (2)	−0.0033 (1)	6.03 (6)	C3	0.3141 (6)	0.2376 (5)	0.2560 (5)	6.0 (2)
P1	0.4744 (2)	0.3258 (1)	0.0939 (1)	3.94 (5)	C3A	0.6974 (7)	0.4741 (6)	0.0849 (5)	7.3 (3)*
P2	0.5072 (1)	0.0723 (1)	0.1974 (1)	3.62 (5)	C3B	0.3951 (6)	0.4776 (6)	0.2442 (5)	6.4 (2)*
F1	−0.0141 (5)	0.1664 (5)	0.2152 (3)	12.6 (2)	C3C	0.4096 (9)	0.3206 (8)	−0.1206 (7)	10.7 (4)*
F2	0.0409 (7)	0.2809 (5)	0.2190 (4)	16.1 (3)	C3D	0.4323 (7)	−0.1043 (6)	0.0567 (5)	7.4 (3)*
F3	−0.0763 (6)	0.2554 (6)	0.1540 (4)	18.5 (3)	C3E	0.7385 (8)	−0.0625 (7)	0.2397 (6)	8.7 (3)*
F4	0.5644 (4)	0.2959 (4)	0.4185 (3)	9.4 (2)	C3F	0.4170 (8)	−0.0286 (7)	0.3777 (6)	8.5 (3)*
F5	0.5483 (4)	0.4184 (4)	0.4047 (3)	9.7 (2)	C4	0.2470 (7)	0.2533 (8)	0.3097 (6)	11.3 (3)
F6	−0.0560 (4)	0.1607 (4)	−0.1374 (3)	10.8 (2)	C4A	0.7648 (7)	0.4241 (6)	0.0669 (6)	7.9 (3)*
O	0.6351 (4)	0.2634 (4)	0.2452 (3)	6.6 (2)	C4B	0.3437 (7)	0.5334 (6)	0.2085 (5)	6.8 (2)*
O1	0.1551 (5)	0.1694 (6)	0.1455 (4)	10.7 (3)	C4C	0.3209 (8)	0.3086 (7)	−0.1186 (6)	9.8 (3)*
O2	0.0833 (7)	0.2713 (4)	0.0688 (4)	13.1 (3)	C4D	0.3400 (7)	−0.1072 (6)	0.0618 (5)	6.8 (2)*
O3	0.3970 (5)	0.2880 (5)	0.4974 (4)	10.7 (2)	C4E	0.8030 (7)	−0.0221((7)	0.2069 (5)	7.8 (3)*
O4	0.3943 (5)	0.4347 (5)	0.4862 (4)	10.2 (2)	C4F	0.4333 (8)	0.0316 (7)	0.4228 (6)	8.7 (3)*
N1	0.3819 (4)	0.1549 (4)	0.0773 (3)	4.5 (2)	C5	0.0223 (6)	0.1288 (5)	0.0615 (4)	5.2 (2)
N2	0.3693 (4)	0.2244 (4)	0.2188 (3)	4.3 (2)	C5A	0.7470 (8)	0.3468 (7)	0.0517 (6)	8.3 (3)*
C	0.5746 (6)	0.2387 (5)	0.2100 (4)	4.6 (2)	C5B	0.3305 (7)	0.5285 (6)	0.1371 (5)	7.4 (3)*
H	0.544 (4)	0.184 (3)	0.108 (3)	6*	C5C	0.2707 (8)	0.3062 (7)	−0.0655 (6)	9.1 (3)*
C1	0.3320 (6)	0.1296 (5)	0.0356 (4)	4.7 (2)	C5D	0.2982 (6)	−0.0603 (5)	0.1069 (5)	5.7 (2)*
C1A	0.5863 (5)	0.3662 (5)	0.0808 (4)	4.6 (2)*	C5E	0.7845 (7)	0.0444 (7)	0.1703 (6)	7.9 (3)*
C1B	0.4188 (5)	0.4070 (5)	0.1375 (4)	4.1 (2)*	C5F	0.4689 (8)	0.1006 (7)	0.4067 (6)	8.6 (3)*
C1C	0.4142 (6)	0.3233 (5)	0.0069 (4)	5.1 (2)*	C6	0.003 (1)	0.2291 (8)	0.1761 (5)	11.3 (4)
C1D	0.4444 (5)	−0.0033 (5)	0.1465 (4)	3.9 (2)*	C6A	0.6579 (7)	0.3175 (6)	0.0612 (5)	7.0 (2)*
C1E	0.6264 (5)	0.0373 (5)	0.2010 (4)	4.2 (2)*	C6B	0.3691 (6)	0.4656 (6)	0.1014 (5)	6.5 (2)*
C1F	0.4739 (5)	0.0550 (5)	0.2870 (4)	4.6 (2)*	C6C	0.3202 (6)	0.3128 (6)	0.0033 (5)	6.7 (2)*
C2	0.2648 (6)	0.0946 (6)	−0.0173 (5)	6.5 (2)	C6D	0.3498 (6)	−0.0081 (5)	0.1496 (4)	5.3 (2)*
C2A	0.6082 (6)	0.4459 (6)	0.0916 (5)	5.9 (2)*	C6E	0.6924 (7)	0.0750 (6)	0.1662 (5)	6.2 (2)*
C2B	0.4322 (6)	0.4135 (5)	0.2095 (4)	5.3 (2)*	C6F	0.4902 (7)	0.1140 (6)	0.3360 (5)	6.8 (2)*
C2C	0.4640 (7)	0.3292 (6)	−0.0521 (6)	7.9 (3)*	C7	0.5027 (6)	0.3530 (6)	0.4179 (5)	6.4 (3)
C2D	0.4870 (6)	−0.0514 (6)	0.0999 (5)	6.1 (2)*					

[a] Values marked with an asterisk indicate that the atoms were refined isotropically. Anisotropically refined atoms are given in the form of the isotropic equivalent thermal parameter defined as $^4/_3[a^2B(11) + b^2B(22) + c^2B(33) + ab(\cos\gamma)B(12) + ac(\cos\beta)B(13) + bc(\cos\alpha)B(23)]$.

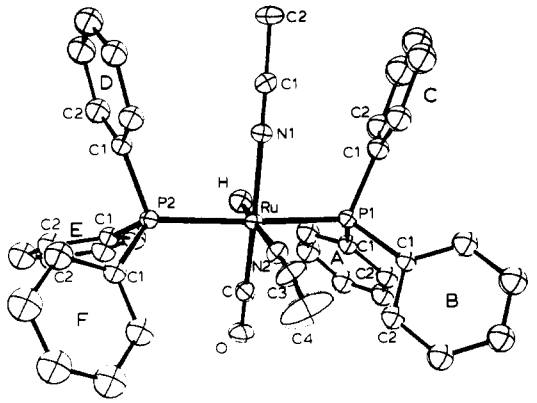

Figure 3. ORTEP drawing of the molecular structure of the cation, $[(Ph_3P)_2RuH(CO)(CH_3CN)_2]^+$, of **6**. Ellipsoids are drawn with 35% probability boundaries.

^{13}C) and $CFCl_3$ (^{19}F) and external 85% H_3PO_4 (^{31}P). Chemical shifts downfield from the reference have positive sign.

Reactions were carried out under nitrogen with use of solvents distilled under nitrogen from appropriate drying agents: toluene (Na–K alloy), acetonitrile (calcium hydride), dimethoxyethane (Na–benzophenone). The fluorochemical acids **1** and **2** were prepared by the method of Koshar and Mitsch.[1]

$[(Ph_3P)_4Ru_2(\mu\text{-}H)_2(\mu\text{-}CF_3SO_2)(CO)_2]HC(SO_2CF_3)_2$ (3). A mixture of 0.91 g (1 mmol) of $(Ph_3P)_3RuH_2(CO)$,[10] 0.56 g of $H_2C(SO_2CF_3)_2$, and 12 mL of toluene was stirred and heated with an 80 °C oil bath for 16 h. Filtration of the reaction mixture in air gave the crude product, which was purified by slow rotary evaporation of a dichloromethane–toluene solution. The yield of brown microcrystals was 0.40 g (47%). Anal. Calcd for $C_{78}H_{63}F_9O_8P_4Ru_3S_3$: C, 54.4; H, 3.7; F, 9.9; P, 7.2; Ru, 11.7; S, 5.6. Found: C, 54.3; H, 3.5; F, 10.1; P, 7.3; Ru, 10.9; S, 5.5. Cyclic voltammetry (in 0.1 M $(n\text{-}C_4H_9)_4NBF_4$ in CH_2Cl_2): reduction wave at –0.82 V vs. SCE; $E_p(ox) - E_p(red)$ is 110 mV at a scan rate of 100 mV/s.

$[(Ph_3P)_4Ru_2(\mu\text{-}H)_2(\mu\text{-}CF_3SO_2)(CO)_2]PhC(SO_2CF_3)_2$ (4). A solution of 4.6 g (5 mmol) of $(Ph_3P)_3RuH_2(CO)$ in 50 mL of toluene was heated to 90 °C (oil bath). A solution of 1.78 g (5 mmol) of $PhCH(SO_2CF_3)_2$ in 10 mL of toluene was added dropwise with stirring during 10 min. After 12 h, the reaction mixture was cooled to room temperature and filtered in air. The solid phase was recrystallized from toluene–dichloromethane to provide, after vacuum-drying, 3.80 g (85%) of **4** as brown microcrystals. Anal. Calcd for $C_{83}H_{67}F_9O_8P_4Ru_2S_3$: C, 55.8; H, 3.8; F, 9.6; P, 7.0; Ru, 11.3; S, 5.4. Found: C, 56.2; H, 3.8; F, 9.6; P, 7.3; Ru, 11.1; S, 5.7.

$[(Ph_3P)_4Ru_2(\mu\text{-}H)_2(\mu\text{-}CF_3SO_2)(CO)_2]Co(CO)_4$ (8). Acetonitrile (15 mL) was added to 0.36 g (0.2 mmol) of **4** and 0.28 g (0.4 mmol) of $PPN^+Co(CO)_4^-$. The mixture was stirred at room temperature for 24 h and then filtered under nitrogen. The solid phase was washed with more acetonitrile and then vacuum-dried to give 0.21 g of **7** as a brown powder. Anal. Calcd for $C_{79}H_{62}CoF_3O_8P_4Ru_2S$: C, 58.5; H, 3.8; Co, 3.5; Ru, 12.5. Found: C, 58.1; H, 3.8; Co, 3.7; Ru, 12.2. IR (Nujol): 1980, 1885 cm^{-1}.

Reaction of $[(Ph_3P)_4Ru_2(\mu\text{-}H)_2(\mu\text{-}CF_3SO_2)(CO)_2]HC(SO_2CF_3)$ with Acetonitrile. Acetonitrile (1.5 mL) was condensed onto 0.3 g of **3**. The resulting solution was heated for 8 h at 85 °C. After the mixture was cooled to room temperature, volatiles were removed on a vacuum line. Their analysis by GC/MS revealed that only acetonitrile was present. A solution of the residue in 6 mL of absolute ethanol deposited, on slow cooling to –20 °C, 0.12 g of white, crystalline **6**. Anal. Calcd for $C_{44}H_{37}F_6N_2O_5P_2RuS_2$: C, 52.1; H, 3.7; F, 11.2; N, 2.8; P, 6.1; Ru, 10.0; S, 6.3. Found: C, 52.0; H, 3.7; F, 11.8; N, 2.7; P, 6.6; Ru, 9.9; S, 6.5.

$(Ph_3P)_4Ru_2(\mu\text{-}H)H_2(\mu\text{-}CF_3SO_2)(CO)_2$ (9). Lithium triethylborohydride (0.3 mL of a 1.0 M solution in tetrahydrofuran) was added by syringe to a stirred suspension of 0.45 g of **4** in dimethoxyethane. After the mixture was stirred for 24 h, the product was isolated by filtration, washed with dimethoxyethane, and vacuum-dried. The yield of dark purple, air-sensitive product was 0.24 g. Anal. Calcd for $C_{77}H_{68}F_3O_5P_4Ru_2S$: C, 62.1; H, 4.6; P, 8.3; Ru, 13.6; S, 2.1; Li, 0.0. Found: C, 62.0; H, 4.6; P, 7.8; Ru, 13.1; S, 2.3; Li, <100 ppm.

X-ray Structure Determinations. Collection and Reduction of X-ray Data. A summary of crystal and intensity collection data for $[(Ph_3P)_4Ru_2(\mu\text{-}H)_2(\mu\text{-}CF_3SO_2]HC(SO_2CF_3)_2\cdot CH_2Cl_2$ (**3**) and $[(Ph_3P)_2RuH(CO)(CH_3CN)_2][HC(SO_2CF_3)_2$ (**6**) is presented in Table V. Crystals of both compounds were secured to the ends of glass fibers with epoxy cement. The crystal class and space group of each compound were determined by use of the Enraf-Nonius CAD4-SDP peak search, centering, and indexing programs[11] and by the systematic absences observed during data collection and were verified by successful solution and refinement. Background counts were measured at both ends of the scan range by using a ω–2θ scan equal, at each side, to one-fourth of the scan range of the peak. In this manner, the total duration of measuring

Table V. Summary of Crystal Data and Intensity Collection

	$3\cdot CH_2Cl_2$	**6**
	Crystal Parameters	
cryst syst	triclinic	monoclinic
space group	$P\bar{1}$ (No. 2)	$P2_1/n$
cryst dimens, mm^3	0.2 × 0.3 × 0.3	0.2 × 0.2 × 0.3
cell params		
a, Å	16.300 (3)	14.561 (3)
b, Å	17.783 (4)	16.858 (3)
c, Å	14.496 (2)	19.122 (4)
α, deg	92.74 (1)	90
β, deg	90.84 (1)	93.55 (2)
γ, deg	111.82 (1)	90
V, Å^3	3910 (2)	4685 (5)
Z	2	4
calcd density, g cm^{-3}	1.636	1.440
temp, °C	23	23
abs coeff, cm^{-1}	6.84	5.46
formula	$C_{89}H_{65}Cl_2F_9O_8P_4S_3Ru_2$	$C_{44}H_{38}F_6N_2O_5P_2S_2Ru_1$
fw	1926.63	1015.94
	Measurement of Intensity Data	
diffractometer	CAD 4	CAD 4
radiation	Mo K$\bar{\alpha}$ (λ = 0.71069 Å)	Mo K$\bar{\alpha}$ (λ = 0.71069 Å)
scan type (2θ range, deg)	ω–2θ (0–46)	ω–2θ (0–50)
no. of unique reflcns		
measd (region)	10564 (+h,+k,l)	8225 (+h,+k,l)
obsd[a]	6874 [$F_o^2 \geq 3\sigma(F_o^2)$]	4018 [$F_o^2 \geq 2\sigma(F_o^2)$]
refinement by full-matrix least squares		
no. of params	606	383
R[b]	0.069	0.059
R_w[b]	0.084	0.063
GOF[b]	1.68	1.99
p[a]	0.03	0.03

[a] The intensity data were processed as described in: "CAD 4 and SDP-PLUS User's Manual"; B. A. Frenz & Assoc., Inc.: College Station, TX, 1982. The net intensity $I = [K(NPI)](C - 2B)$, where K = 20.1166 × attenuator factor, NPI = ratio of fastest possible scan rate to scan rate for the measurement, C = total count, and B = total background count. The standard deviation in the net intensity is given by $[\sigma(I)]^2 = (K/NPI)^2[C + 4B + (pI)^2]$, where p is a factor used to downweight intense reflections. The observed structure factor amplitude F_o is given by $F_o = (I/Lp)$, where Lp = Lorentz and polarization factors. The $\sigma(I)$'s were converted to the estimated errors in the relative structure factors $\sigma(F_o)$ by $\sigma(F_o) = [\sigma(I)/I]F_o$. [b] The function minimized was $\sum w(|F_o| - |F_c|)^2$, where $w = 1/[\sigma(F_o)]^2$. The unweighted and weighted residuals are defined as $R = (||F_o| - |F_c||)/\sum|F_o|$ and $R_w = [(\sum w(|F_o| - |F_c|))^2/(\sum w|F_o|)^2]^{1/2}$. The error in an observation of unit weight (GOF) is $[\sum w(|F_o| - |F_c|)^2/(NO - NV)]^{1/2}$, where NO and NV are the numbers of observations and variables, respectively.

(10) Ahmad, N.; Levison, J. J.; Robinson, S. D.; Uttley, M. F. *Inorg. Synth.* **1974**, *15*, 45.

(11) All calculations were carried out on PDP 8A and 11/34 computers with use of the Enraf-Nonius CAD4 SDP-PLUS programs. This crystallographic computing package is described by: Frenz, B. A. In "Computing in Crystallography"; Schenk, H., Olthof-Hazekamp, R., van Konigsveld, H., Bassi, G. C., Eds.; Delft University Press: Delft, Holland, 1978; Pp 64–71. Frenz, B. A. In "Structure Determination Package and SDP-PLUS User's Guide"; B. A. Frenz Associates: College Station, TX, 1982.

backgrounds was equal to half of the time required for the peak scan. The intensities of three standard reflections were measured every 1.5 h of X-ray exposure time for both compounds, and no decay with time was noted. The data were corrected for Lorentz, polarization, and background effects. The effects of absorption were not significant as judged by empirical ψ-scan data[11] (less than 3% in intensity), and therefore absorption corrections were not applied.

Solution and Refinement. The structures were solved by conventional heavy-atom techniques. The Ru atoms were located by Patterson syntheses. Full-matrix least-squares refinement and difference Fourier calculations were used to locate all remaining non-hydrogen atoms. The atomic scattering factors were taken from the usual tabulation,[12] and the effects of anomalous dispersion were included in F_c by using Cromer and Ibers'[13] values of $\Delta f'$ and $\Delta f''$. For compound **6** the positions of the phenyl and anion hydrogen atoms were calculated with use of the program HYDRO[1] (C–H distance set at 0.95 Å) and included in the structure factor calculations but were not refined. The Ru hydride in **6** was located by difference Fourier analysis. The positional parameters of the hydride were refined, but its thermal parameter was fixed. In compound **3**, the Ru hydrides were not located. The bridging SO_2CF_3 group was found to be disordered such that the S1, C3, and F3 atoms had two positions each with a 50% occupancy. The two positions, labeled primed and unprimed, were refined to give reasonable distances and angles. The two positions found for the bridging SO_2CF_3 correspond to isomers that result from tilting of the SCF_3 group in different directions. Only one of the two isomers is shown in Figure 2. Compound **3** was found to have a CH_2Cl_2 solvate molecule. As usual, this molecule was somewhat disordered and probably had partial occupancy. The distances and angles after refinement gave reasonable values. The final difference Fourier maps for both compounds did not reveal any significant residual electron density. The final positional and thermal parmeters of the refined atoms are given in Tables II and III and as supplementary material. Tables of observed and calculated structure factor amplitudes are inclined as supplementary material. ORTEP views of both compounds are shown in Figures 2 and 3 and as supplementary material.[5]

Acknowledgment. The authors are grateful to members of the 3M Analytical and Properties Research Laboratory for the spectroscopic and analytical data and to Robert Koshar, 3M Industrial and Consumer Sector Research Laboratory, for gifts of fluorocarbon acids. The 600-MHz ^{1}H NMR spectra were obtained at the Carnegie-Mellon University NMR Facility for Biomedical Studies. L.H.P. acknowledges support by the National Science Foundation for his contribution to this work.

Registry No. **1**, 428-76-2; **2**, 40906-82-9; **3**, 101011-69-2; **4**, 101141-60-0; **5**, 101011-70-5; **6**, 101011-71-6; **6a**, 101011-73-8; **8**, 101141-61-1; **9**, 101011-74-9; $(Ph_3P)_3RuH_2(CO)$, 25360-32-1; Ru, 7440-18-8.

Supplementary Material Available: Tables of distances and angles, general temperature factor expansions, least-squares planes, and observed and calculated structure factor amplitudes for **3** and **6**, a table of positional parameters for hydrogen atoms in **6**, ORTEP views of the $HC(SO_2CF_3)_2^-$ anions in **3** and **6**, and an ORTEP stereoview of the cation in **3** (66 pages). Ordering information is given on any current masthead page.

(12) Cromer, D. T.; Waber, J. T. "International Tables for X-Ray Crystallography"; Kynoch Press: Birmingham, England, 1974; Vol. IV, Table 2.2.4. Cromer, D. T. *Ibid*, Table 2.3.1.
(13) Cromer, D. T.; Ibers, J. A. In ref 12.

Contribution No. 7201 from the Arthur Amos Noyes Laboratory, California Institute of Technology, Pasadena, California 91125

Photophysics and Electrochemistry of Hexanuclear Tungsten Halide Clusters

Thomas C. Zietlow, Daniel G. Nocera, and Harry B. Gray*

Received May 30, 1985

The $W_6X_{14}^{2-}$ (X = Cl, Br, I) clusters possess emissive excited states characterized by microsecond lifetimes and large emission quantum yields (up to 0.39). The energy of the emissive state increases according to $W_6Cl_{14}^{2-}$ (1.83 eV) < $W_6Br_{14}^{2-}$ (1.85 eV) < $W_6I_{14}^{2-}$ (2.05 eV), which is the opposite trend from that expected when charge-transfer character is mixed into a primarily metal-localized transition. Variable-temperature emission data have been collected for the $(TBA)_2W_6X_8Y_6$ (Y = Cl, Br, I) clusters, indicating that the bridging halides (X) primarily determine the excited-state energy. The one-electron-oxidation potentials of the clusters also reflect the dominant electronic structural role of the bridging halides. The terminal halides (Y) have a substantial effect on the nonradiative decay rate, with k_{nr} decreasing according to Cl > Br > I.

Much of our work in inorganic photochemistry has centered on hexanuclear d^4 clusters, $M_6X_{14}^{2-}$ (M = Mo, W; X = Cl, Br, I), which feature long-lived excited states and several accessible oxidation levels.[1] On the basis of studies of the luminescences of $Mo_6Cl_{14}^{2-}$, $Mo_6Br_{14}^{2-}$, and $W_6Cl_{14}^{2-}$, we have suggested that the electronic transition that takes the emissive state to the ground state is primarily localized on the metal cluster core.[2] Further work has confirmed that a metal-localized description is correct for the $Mo_6X_{14}^{2-}$ series,[3] but the emissive behavior of the analogous tungsten clusters is more complicated.[4,5] In order to probe ligand effects on cluster properties more thoroughly, we have prepared the mixed halides $W_6X_8Y_6^{2-}$ (Y = Cl, Br, I) and have investigated their photophysical and electrochemical behavior.

Table I. Emission Data[a]

complex	λ_{max}, nm	τ, μs	ϕ_{em}	$10^{-4}k_r$, s^{-1}	$10^{-4}k_{nr}$, s^{-1}
$(TBA)_2W_6Cl_{14}$	833	1.5	0.02	1.3	65
$(TBA)_2W_6Cl_8Br_6$	814	2.3	0.04	1.7	42
$(TBA)_2W_6Cl_8I_6$	802	3.0	0.07	2.3	31
$(TBA)_2W_6Br_8Cl_6$	766	9.7	0.10	1.0	9.3
$(TBA)_2W_6Br_{14}$	758	15	0.15	1.0	5.7
$(TBA)_2W_6Br_8I_6$	752	15	0.25	1.7	5.0
$(TBA)_2W_6I_8Cl_6$	701	10	0.11	1.1	8.9
$(TBA)_2W_6I_8Br_6$	698	22	0.25	1.1	3.4
$(TBA)_2W_6I_{14}$	698	30	0.39	1.3	2.0

[a] Recorded in acetonitrile solution at 21 ± 2 °C; TBA = $(n\text{-}C_4H_9)_4N$.

Experimental Section

Cluster Compounds. $[(n\text{-}C_4H_9)_4N]_2Mo_6Cl_{14}$, $[(n\text{-}C_4H_9)_4N]_2Mo_6Br_{14}$, and $[(n\text{-}C_4H_9)_4N]_2W_6Cl_{14}$ were prepared as described previously.[2] The other $[(n\text{-}C_4H_9)_4N]_2W_6X_{14}$ clusters were obtained from alkali metal

(1) Maverick, A. W.; Gray, H. B. *J. Am. Chem. Soc.* **1981**, *103*, 1298.
(2) Maverick, A. W.; Najdzionek, J. S.; MacKenzie, D.; Nocera, D. G.; Gray, H. B. *J. Am. Chem. Soc.* **1983**, *105*, 1878.
(3) Zietlow, T. C.; Nocera, D. G.; Gray, H. B., unpublished observations.
(4) Zietlow, T. C.; Hopkins, M. D.; Gray, H. B. *J. Solid State Chem.* **1985**, *57*, 112.
(5) Zietlow, T. C.; Schaefer, W. P.; Sadeghi, B. S.; Hua, N.; Gray, H. B. *Inorg. Chem.*, in press.

0020-1669/86/1325-1351$01.50/0